Supplementary Information

Bioinspired magnetism-responsive hybrid microstructures with dynamic switching toward liquid droplet rolling states

Yucheng Bian [a#], Suwan Zhu [a#], Xin Li [b*], Yuan Tao [a], Chenyu Nian [a], Chenchu Zhang [c], Yubin Peng [d], Chuanzong Li [e], Wei Xiong [f], Wulin Zhu [a], Yanlei Hu [a], Jiawen Li [a], Jiaru Chu [a] and Dong Wu [a*]

[a]*CAS Key Laboratory of Mechanical Behavior and Design of Materials, Department of Precision Machinery and Precision Instrumentation, University of Science and Technology of China, Hefei, Anhui 230027, China.*

[b]*State Key Laboratory of Pulsed Power Laser Technology College of Electronic Engineering, National University of Defense Technology, Hefei, Anhui 230000, China.*

[c]*Anhui Province Key Lab of Aerospace Structural Parts Forming Technology and Equipment, Institute of Industry & Equipment Technology, Hefei University of Technology, Hefei, Anhui 230009, China.*

[d]*School of Mechanical and Electrical Engineering, Anhui Jianzhu University, Hefei, Anhui 230601, China.*

[e]*School of Computer and Information Engineering, Fuyang Normal University, Fuyang, Anhui 236037, China.*

[f]*Wuhan National Laboratory for Optoelectronics, Huazhong University of Science and Technology, Wuhan, Hubei 430074, China.*

**Corresponding author*

E-mail: lixinkiller@nudt.edu.cn (Xin Li)

E-mail: dongwu@ustc.edu.cn (Dong Wu)

[#]*These authors contributed equally.*

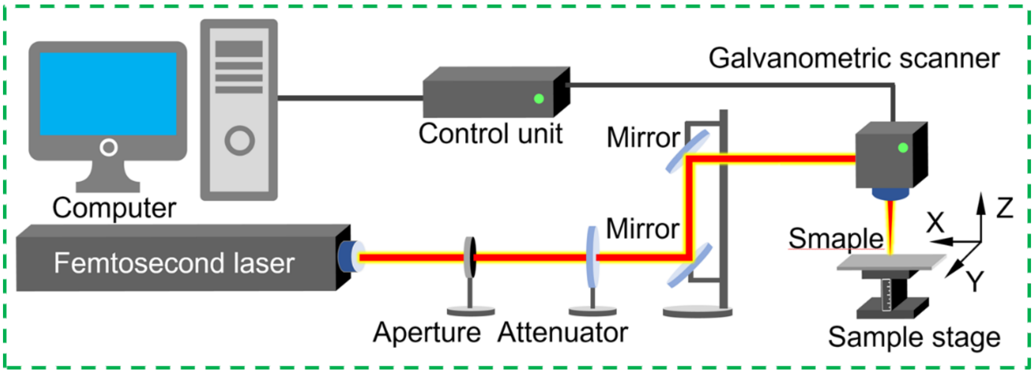

Fig. S1 Femtosecond laser processing system and optical path in GMRMA preparation.

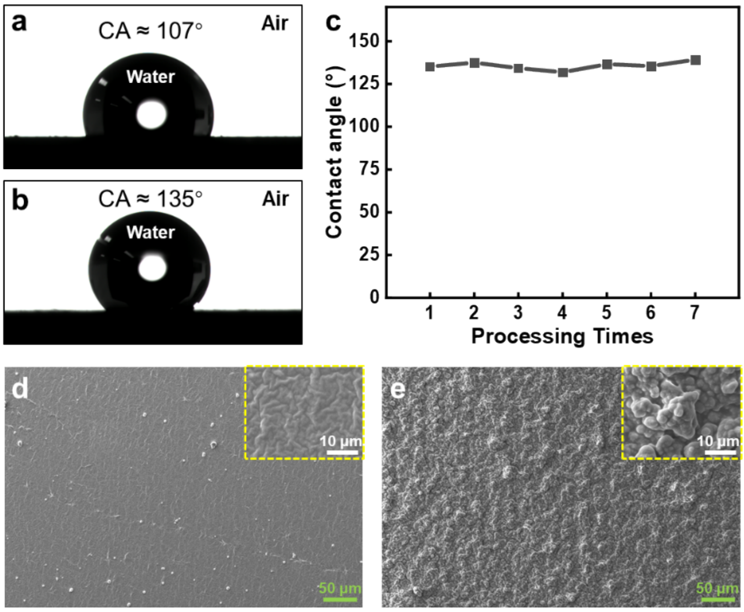

Fig. S2 Femtosecond laser surface modification to improve the hydrophobicity of GMRMA. (a) The surface water contact angle (WCA) of the cured hybrid colloid before laser scanning was ~107°. (b) After one fast laser scanning, the WCA increased to ~135°. (c) The graph suggests that multiple modifications do not keep improving the hydrophobicity. (d) Planar scanning electron microscope (SEM) image of the cured hybrid colloid before laser scanning. (e) SEM image of the cured hybrid colloid after laser scanning.

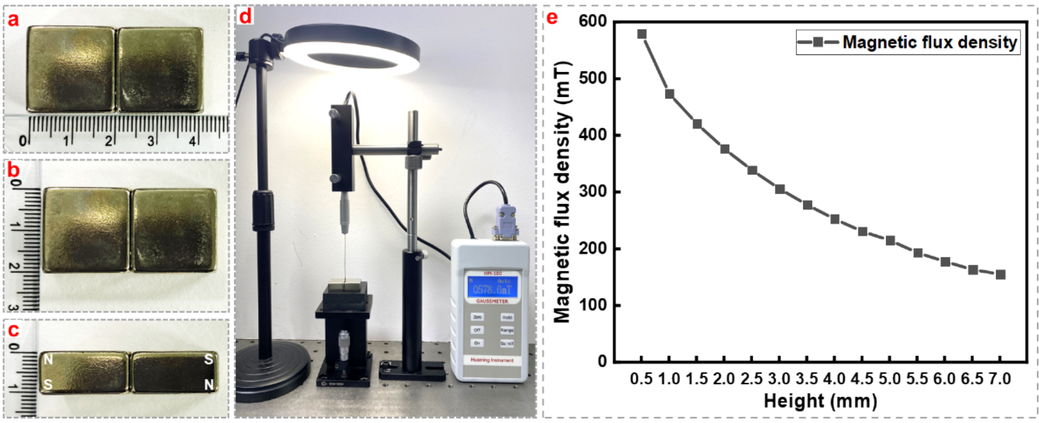

Fig. S3 Two NdFeB permanent magnets that attract each other are shown with (a) length, (b) width and (c) height respectively, and GMRMA is placed at the junction of two permanent magnets, which can realize the bending deformation of micropillars. (d) Experimental setup for measuring the magnetic flux density above the magnets junction. (e) The magnetic flux density at different heights above the magnets junction. The GMRMA sample structure was located ~1.5mm above the junction, where the magnetic flux density was ~400 mT.

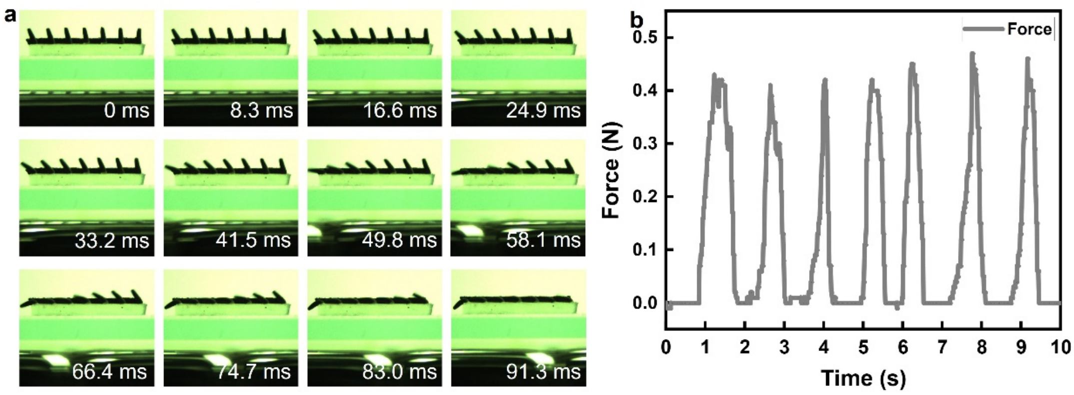

Fig. S4 The equivalent magnetic bending force and conversion time were quantified as GMRMA transformed from isotropic state to anisotropic state. (a) A typical seven-micropillar array completely bent at approximately t = 91.3 ms. The magnetic flux density was set as ~ 400 mT in the vicinity of the bent micropillars. (b) An increasing pressure was loaded on the upper surface of a 15×8 micropillar array. The total bending force was measured as ~0.43 N, indicating a transition force of approximately 3.58 mN on a single micropillar.

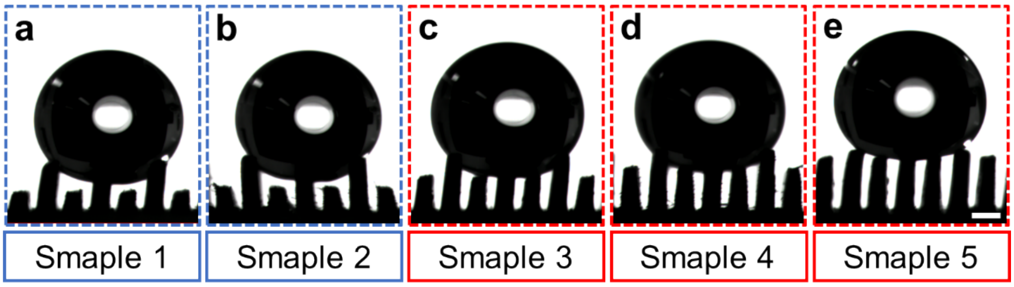

Fig. S5 Interfacial contact configurations of sample 1 to 5 when magnetic field is off. The microplate structures of (a) sample 1 and (b) sample 2 are not in contact with the droplet, and the samples show favorable isotropic wettability. The microplate structures of (c) sample 3, (d) sample 4 and (e) sample 5 are in contact with the droplet, and the samples do not have isotropic wettability. Scale bar = 500 μm.

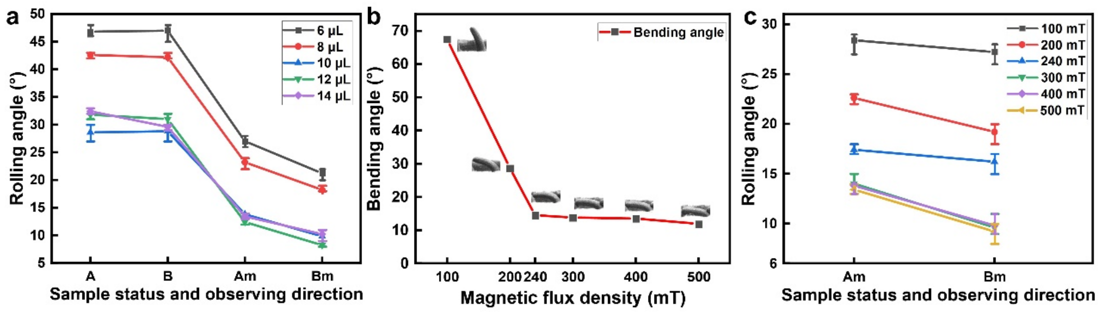

Fig. S6 (a) Impact of droplet size (volume) and magnetic flux density on GMRMA anisotropy. Five droplet volumes (6, 8, 10, 12, 14 μL) were employed here. It is shown that GMRMA exhibited a favorable tolerance for isotropic/anisotropic droplet rolling shift in different sizes. (b) and (c) A minimum value of ~100 mT was observed during the micropillars bending process. At this stage, GMRMA started to show droplet rolling anisotropy. When the magnetic flux density exceeded ~240 mT, the height of the bent micropillars became lower than the microplates, the droplet rolling anisotropy tended to be stable and finally reached extrema beyond 300 mT.

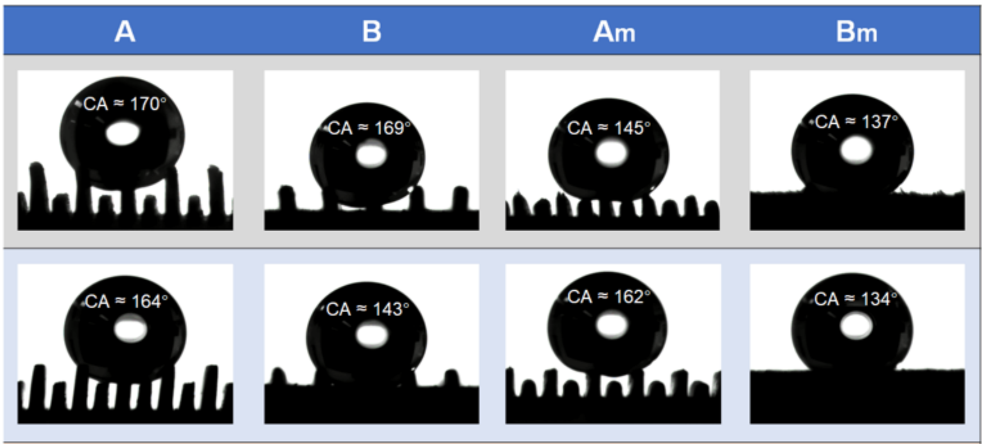

Fig. S7 Static contact angle variation on two typical samples (samples 2 and 3). It is observed that the difference of static contact angles along A and B directions enlarged for both samples as the magnetic field was applied, which in turn validated the enlarged anisotropic energy barriers along the two orthogonal directions.

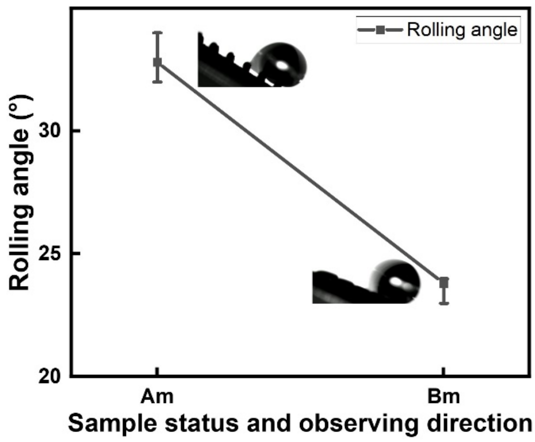

Fig. S8 The anisotropic rolling characteristics of droplets were observed on a pure micropillar-array along A and B directions under magnetic force stimulus (Am and Bm).

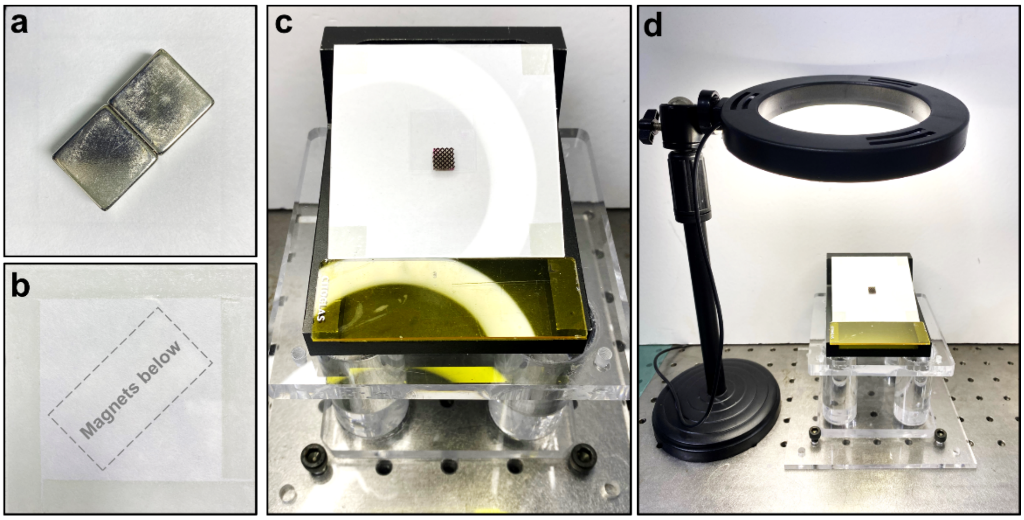

Fig. S9 Photographs of reconfigurable micro-droplet guiding system. (a) back and (b) front of the sample platform. The magnets behind the sample platform were placed at 45°. (c) and (d) show the experimental setup of the home-made reconfigurable droplet guiding system.